

Methods for photophysical characterization of red fluorescent proteins at the single-molecule level

Emma Simmerman

An honors thesis submitted to the
University of Colorado in partial fulfillment
of the requirements for departmental honors

Bachelor of Arts

Department of Physics

2019

This thesis entitled:

*Methods for photophysical characterization of red fluorescent proteins at the
single-molecule level*

written by

Emma M. Simmerman

has been approved for the Department of Physics

Thesis defense: April 8, 2019

Thesis advisor: Ralph Jimenez (Department of Chemistry and Biochemistry, JILA)

Honors council representative: Jun Ye (Department of Physics, JILA)

Committee member: Tobin Munsat (Department of Physics)

Abstract: The ability to monitor cellular processes at high resolution using genetically encodable fluorescent protein tags and sensors has revolutionized life science research. In particular, several super-resolution imaging techniques take advantage of the phenomenon of stochastic fluorescent protein blinking. Here we present a method for measurement and analysis of the blinking behavior of red fluorescent proteins. This project contributes to the characterization of crucial photophysical parameters of fluorescent proteins used for super-resolution imaging techniques.

Acknowledgements

I am deeply grateful for the support and encouragement I have received during my time in the Jimenez group. Thank you to Dr. Sheng Ting Hung and Srijit Mukherjee, for spending untold hours answering my never-ending questions, and sharing your snacks. Thank you to Samantha Allen, Kristen Parzuchowski, Dr. Alex Mikhaylov, Dr. Josh Slocum, and Dr. Nancy Douglas, for your perpetual kindness and willingness to help. Finally, I am grateful to Professor Ralph Jimenez for welcoming me into his group, where I have learned a bit about how to be a scientist.

I am grateful to friends in Boulder, including Nate Nickrent, Katherine Rose, Paul Reynerson, Olivia Treitman, Kyle Kolanowski, Syd Levy, Tristan Davolt, Andres Mora, Lisa Wang, and Marc Thomson, who have each shaped my journey in countless ways.

I am grateful to my parents and step-parents and to my siblings, for their unwavering belief in my potential.

Thank you so very much.

Contents

1	Introduction	1
1.1	Fluorescent proteins	1
1.2	Red and near-infrared fluorescent proteins of interest	2
1.3	Fluorescent protein photophysics	3
1.4	Applications in super-resolution imaging	6
1.5	Ensemble fluorescence measurements	8
1.6	Single-molecule fluorescence measurements	9
2	Experimental Methods	10
2.1	Ensemble measurements of photobleaching	10
2.2	Single molecule measurements	11
2.2.1	Sample preparation and single molecule imaging	11
2.2.2	Data analysis	15
3	Results and discussion	19
3.1	Ensemble fluorescence measurements	19
3.2	Single-molecule fluorescence measurements	19
3.3	Conclusion and future directions	21

1 Introduction

1.1 Fluorescent proteins

Since the first demonstration in [1] of a genetically encoded biosensor utilizing green fluorescent protein (GFP), fluorescent proteins (FPs) have become crucial tools in numerous applications spanning the disciplines of biological science [2] [3]. Most FPs are less cytotoxic than dyes, and fluoresce without added coenzymes [4]. Using standard molecular biology techniques, an FP-encoding sequence can be inserted nearly arbitrarily into the DNA of any organism, allowing for minimally intrusive fluorescent labeling of virtually any target protein [5]. Common applications of FPs include the quantification and tracking of target protein populations *in vivo*, and the monitoring of cellular conditions over time. For example, cell cycle transitions in tumor cells have been visualized by tagging structural elements [6], and linked FPs which participate in Förster resonant energy transfer (FRET) are commonly used as indicators of intracellular parameters such as pH, temperature, voltage, mechanical stress, and levels of organic and inorganic signalling molecules [7] [8]. The generic structure of a monomeric FP consists of a β barrel surrounding a light-sensitive chromophore (Fig. 1), though FPs originally isolated from different species can vary considerably in structure.

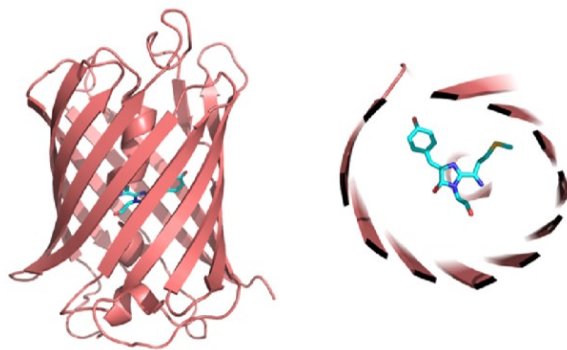


Figure 1: Crystal structure of the commonly used red FP mCherry (Protein Data Bank ID: 2H5Q), consisting of an 11-stranded β barrel with a chromophore formed by the condensation of an XYG tripeptide [9].

higher fluorescence lifetime and improved brightness [13]. The blinking behavior of FR has been demonstrated to work in super-resolution imaging of live cells [14], but the crucial photophysics controlling its performance have not been characterized, limiting the generalization of these results. In the future, the techniques developed here for characterization of RFP photophysics at the single-molecule level can be expanded to other RFPs of interest.

1.3 Fluorescent protein photophysics

A rainbow of FPs now exist with a wide variety of photophysical properties such as photostability, excited state lifetime, quantum yield, extinction coefficient, and excitation and emission spectra (as well as relevant biological parameters such as cytotoxicity, maturation speed, pH and O₂ sensitivity, and oligomerization) [15]. In practice, all of these parameters contribute to a researcher’s choice of FP to use in a particular application and must be well-characterized.

Brightness is one of the most important characteristics of an FP, but the cellular environment can alter photophysics, so that cellular and molecular brightness are different in general. The theoretical molecular brightness (B) of an FP is simply given by Eq. (1), where Φ is the fluorescence quantum yield and ϵ is the extinction coefficient [16].

$$B = \Phi \times \epsilon \tag{1}$$

Quantum yield is the fraction of photons emitted compared to photons absorbed, and thus is a measure of the extent to which non-radiative processes contribute to depopulation of the excited state. The extinction coefficient can be converted to the absorption cross section of the FP molecule, and is a wavelength-dependent constant representing the capacity of the fluorophore to absorb radiation [10].

The processes resulting from perturbation of an FP with visible light can be illustrated by a simple 3-state model (Fig. 3). At room temperature, the vast majority of FP chromophores occupy the ground state (S_0), as dictated by the Boltzmann distribu-

tion [17]. Upon absorption of a photon of appropriate energy, a transition can occur to the first excited state (S_1). From here the system can either relax directly to the ground state by emitting a photon (the phenomenon of fluorescence), or non-radiatively by internal conversion. The system might also undergo a non-radiative transition to a dark state (D). The chemical nature of the dark state varies with different fluorophores. In some systems, the dark state has been characterized as a cis/trans isomer [18], a differently protonated or radical form [19], or a triplet state [20]. The non-radiative transition from S_1 to D is here called dark state conversion (DSC), and non-radiative relaxation from D to S_0 is called ground state recovery (GSR). It should be noted that vibrational relaxation to the lowest vibrational level of each molecular energy level also occurs; however, the timescale for such vibrational relaxation is typically fast compared to other transitions, so this process is neglected here.

During irradiation, the cycle of excitation, emission, internal conversion, dark state conversion, and ground state recovery continues until the fluorophore undergoes an irreversible conformational change or reaction to a state which can no longer fluoresce. This process is termed irreversible photobleaching, which can take place from both the excited and the dark state; however, in the lower irradiance regimes of this experiment, the FP will spend less time in S_1 on average, making the main photobleaching contribution from D .

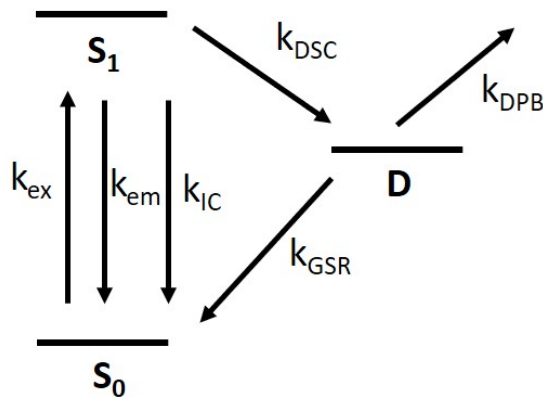


Figure 3: Simple 3-state diagram for ground (S_0), first excited (S_1), and dark (D) states. Vibrational and rotational energy states not shown.

At the ensemble level, the presence of a dark state leads to a fast decay component in the measured fluorescence, as the excited state population decreases due to DSC. At the single-molecule level, the presence of a dark state gives rise to a blinking phenomena, where the cycle of excitation and emission between S_0 and S_1 (the "on" state) is interrupted by a transition to D (the "off" state). Single-molecule blinking was first observed for GFP [21]. A fluorescent signal trace from this seminal experiment is shown in Fig. 4.

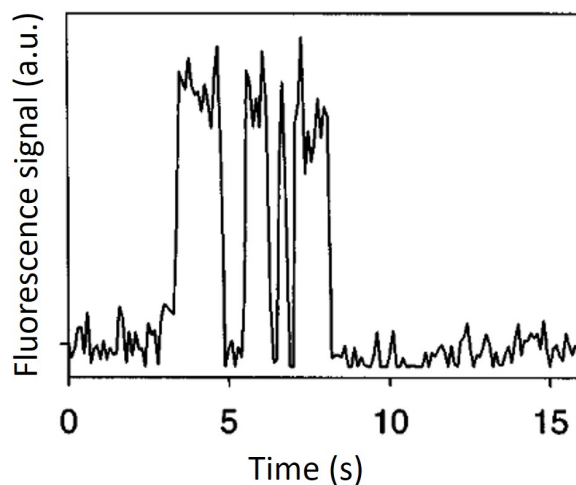


Figure 4: First observed single-molecule blinking in GFP (adapted from [21])

In Fig. 3, the chemical rate constants of each transition process are shown as arrows. Each rate constant is proportional to the corresponding transition probability [22]. Thus, assuming first-order kinetics, the rate equations describing the populations of these states are given in Eq. (2)

$$\begin{aligned}
 \frac{dn_{S_0}}{dt} &= -k_{ex}n_{S_0} + (k_{IC} + k_{em})n_{S_1} + k_{GSR}n_D \\
 \frac{dn_{S_1}}{dt} &= k_{ex}n_{S_0} - (k_{em} + k_{IC} + k_{DSC})n_{S_1} \\
 \frac{dn_D}{dt} &= k_{DSC}n_{S_1} - (k_{GSR} + k_{DPB})n_D
 \end{aligned}
 \tag{2}$$

where n_{S_0} , n_{S_1} , and n_D are the ground, excited, and dark state populations and k_{em} , k_{ex} , k_{DSC} , k_{IC} , and k_{GSR} are the rate constants of emission, excitation, dark state conversion, internal conversion, and ground state recovery, respectively. The total pop-

ulation ($n_{S_0} + n_{S_1} + n_D$) remains constant. These parameters can be calculated from experimental conditions, photophysical measurements, and fits of experimental ensemble fluorescence data. The excitation rate k_{ex} is proportional to the illumination irradiance and extinction coefficient of the fluorophore. The internal conversion rate k_{IC} is given by solving Eqs. 3, where τ_{ex} is the excited state lifetime.

$$\begin{aligned}\tau_{ex} &= \frac{\Phi}{k_{ex}} \\ \tau_{ex} &= \frac{1}{k_{em} + k_{IC}}\end{aligned}\tag{3}$$

For a 3-state model, the relationship between these rate constants and the average blinking on and off time intervals (τ_{ON} and τ_{OFF}) is given by Eq. (4) [23].

$$\begin{aligned}\frac{1}{\tau_{ON}} &= \frac{k_{ex} \times k_{DSC}}{k_{em} + k_{IC} + k_{DSC}} \\ \frac{1}{\tau_{OFF}} &= k_{GSR}\end{aligned}\tag{4}$$

1.4 Applications in super-resolution imaging

The wave nature of light causes diffraction when radiation is incident upon a lens, so that the image of a point is not point-like, but rather a blur [24]. This gives rise to the Abbe diffraction limit, a minimum distance at which two points which can be resolved by optical microscopy. The approximate expression for this distance d is given in Eq. (5) for incoherent illumination, where λ is the wavelength of illumination in vacuum, n is the index of refraction of the medium surrounding the lens, and θ is the angle from which rays of light from the point reach the outer edge of the imaging lens [25]. The quantity $n \sin \theta$ is defined as the numerical aperture of the lens.

$$d \approx 0.61 \frac{\lambda}{n \sin \theta}\tag{5}$$

For typical microscope lenses and visible light, the diffraction limit is about 200 nm.

Various optical microscopy techniques have been developed in recent decades to overcome the diffraction barrier and achieve super-resolution. The discussion here will be limited to several which harness the properties of photoactivatable FPs (PAFPs), which change fluorescent states upon irradiation of specific wavelength and intensity. Possible changes include activation from a non-fluorescent to fluorescent state, irreversible photoconversion to fluoresce at a new wavelength, and reversible switching between fluorescent states [26].

The basis of each of these techniques is the ability of fluorescent probes to switch and be switched between "on" and "off" states. Temporal resolution of fluorescence events can be obtained and converted to spatial resolution by tuning illumination conditions so that only a small part of the population is in the on state at a time. Thus the fluorescence collected from each diffraction-limited spot is assumed to come from a single molecule, the location of which is further resolved by statistical analysis of the point-spread function.

In 2006, three groups independently developed super-resolution techniques which involve active conversion of fluorescent probes between fluorescent states. In photoactivated localization microscopy (PALM), small subsets of the population of PAFPs in a sample are successively switched to a fluorescent state and then photobleached, by modulation of the illuminating laser pulse intensity and duration [27]. The approach of fluorescence photoactivated localization microscopy (fPALM) is similar, but imaging is carried out on a traditional confocal microscope system [28], while PALM utilizes total internal reflection fluorescence microscopy (discussed in section 2.2.1). Similarly, sub-diffraction-limit imaging by stochastic optical reconstruction microscopy (STORM) involves successive photoactivation and deactivation of small subpopulations of fluorescent dye molecules using radiation of different wavelengths [29].

These techniques are capable of enhancing spatial resolution down to tens of nanometers [30], at the expense of temporal resolution. Running enough cycles of controlled photoactivation and deactivation to construct an image requires minutes of acquisition time [31]. In contrast, super-resolution optical fluctuation imaging (SOFI) is

a technique which relies on spontaneous reversible photoswitching between fluorescent states, so the acquisition rate is in principle limited only by the intrinsic timescale of the fluorophore's switching [32]. Thus the goal of the present study is to characterize the photophysics of FPs which exhibit spontaneous "blinking" as they switch from off to on and back. These FPs are well-suited to super-resolution techniques such as SOFI.

1.5 Ensemble fluorescence measurements

Ensemble measurements of FPs involve measuring fluorescence emitted over time from a large number of FP molecules. The observed fluorescent decay results from depopulation of the S_1 state by all radiative and non-radiative processes, and the shape of the decay gives insight into the rates of these processes. Fluorescence decay patterns vary from simple mono- and multiexponential decay curves to transient increases or decreases, eventually followed by decay, and vary depending on the FP, intensity regime, and temporal illumination pattern [33].

Information is extracted by fitting the fluorescence traces according to a model as in Fig. 3. Ensemble measurements on purified protein and *E. coli* using continuous and pulsed illumination in the time and frequency domains have been used to extract DSC and GSR rate constants for various RFPs [33][34]. However, these measurements in the 100 W/cm²- 100 kW/cm² irradiance regime are far from the 1-10s of W/cm² regime of typical biological imaging conditions, and the extrapolation of these parameters to lower irradiance regimes is not trivial [35]. The ultimate goal of the present study is to characterize DSC and GSR in these low irradiance regimes relevant for imaging applications.

In this experiment, ensemble measurements were performed on FPs in *E. coli* without the temporal resolution necessary to discern details of fluorescence decay at μ s timescales as reported in [33]. However, at low enough intensities, permanent photobleaching processes are slow, so that the decay consists of clearly differentiated fast and slow decay process (discussed in section 3.1). The fast component roughly corresponds to GSR [33], typically the limiting process in fluorescence recovery, and the slow

component is due to permanent photobleaching. At higher intensities, photobleaching occurs faster, and these two decays occur on comparable timescales. In this experiment, ensemble measurements were performed to qualitatively estimate the timescales of GSR and permanent photobleaching, and find an irradiance regime at which the decay due to photobleaching is much slower than the fast decay. In this regime, curve fittings and simulations based on the 3-state model in Fig. 3 can be done while neglecting photobleaching, a difficult parameter to estimate and an undesirable process in real imaging applications. The DSC and GSR rate constants can then be calculated by fitting the ensemble data to the analytic solution of Eq. 2 without considering photobleaching. The analytic solution is a complicated vector function of all of the rate constants and time. k_{DSC} and k_{GSR} values obtained in this way can then be used to predict average on and off times, which can be observed from single molecule imaging, according to Eq. 4.

1.6 Single-molecule fluorescence measurements

The first successful demonstrations of single-molecule optical imaging began nearly three decades ago, first using laser frequency double modulation techniques to observe single pentacene dopant molecules in a crystal matrix at cryogenic temperature [36]. Shortly thereafter, individual fluorescent dye molecules were observed in solution [37]. Since then, SM imaging techniques have been used to elucidate the mechanisms of various cellular processes.

SM studies provide the same information about average transition rates as ensemble measurements, with additional insight into time-dependent processes and possible heterogeneity of molecule populations which must be assumed in ensemble measurements to be homogeneous. In SM studies, stochastic "quantum jumps" between radiative and non-radiative electronic states can be directly observed as abrupt interruptions in fluorescence [20], a process which is more difficult to probe at the ensemble level (though it can be done [34]), where the transitions of individual molecules are not synchronized. From SM studies, frequency histograms can be constructed, show-

ing the full distribution of a measured parameter. Multiple peaks and skewing of the distribution can indicate the presence of heterogeneous subpopulations. In biological contexts such as FPs, where different folded configurations give rise to differing spectral properties, detecting heterogeneity is especially critical [38].

Fluorescent molecules have been shown to give better signal-to-background ratio than the first optical SM techniques involving sophisticated laser modulation, because emitted photons are red-shifted, and can thus be effectively distinguished by long-pass filters from the excitation beam [38]. Still, achieving maximum signal-to-background is the main challenge of SM fluorescence spectroscopy. Background noise comes from a variety of sources, including scattering from optical components, detector dark count, residual unfiltered excitation radiation, and fluorescence from the solvent and impurities [38].

2 Experimental Methods

2.1 Ensemble measurements of photobleaching

Ensemble measurements of FR in the bacteria *E. coli* were done to obtain the rate constants of dark state conversion and ground state recovery. The plasmid DNA of FR was transformed into and expressed in *E. coli* cells and grown for 45-60 minutes in LB media in a shaker at 37 °C and 230 rpm. The culture was plated on an agar plate with ampicillin resistance and arabinose for overnight expression in an incubator at 37 °C. Colonies which showed bright color were chosen from plates. 2-3 colonies were mixed with 500 μ L imaging buffer (150 mM HEPES, 100 mM NaCl, pH 7.4) by vortexing for no longer than 20 s. A glass coverslip and glass slide were cleaned with Alconox detergent, rinsed with deionized water, and blown dry with filtered compressed air. 9 μ L of the mixture were added between the coverslip and glass slide, which formed a sample chamber.

The sample was imaged on an Olympus IX73 inverted microscope system (Fig. 5). It was excited by 561 nm continuous wave laser illumination (Toptica) and im-

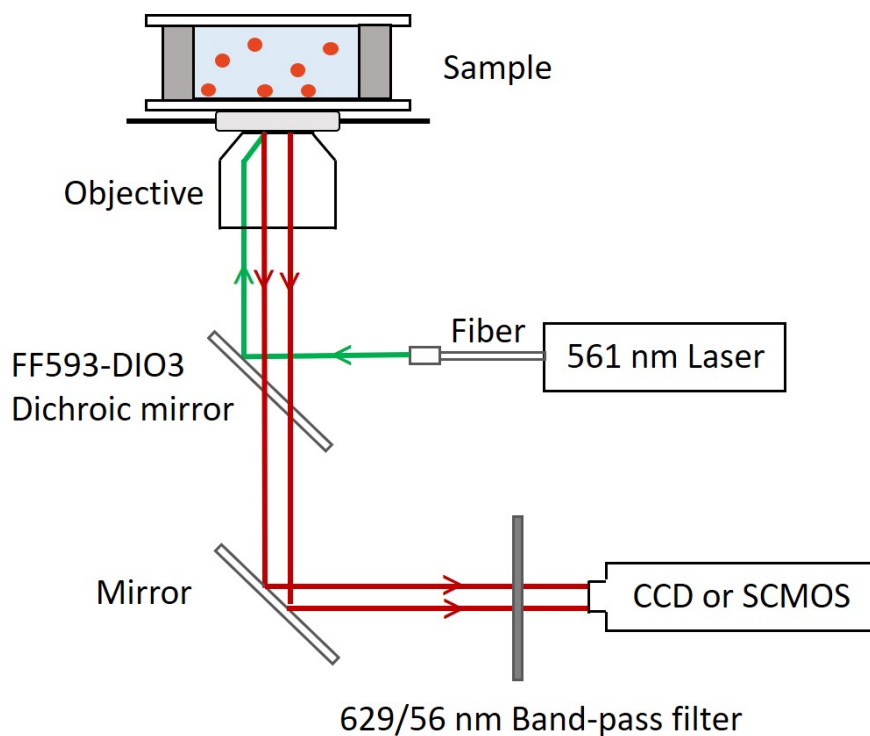


Figure 5: Olympus IX73 inverted microscope system with which ensemble and single-molecule measurements were taken.

aged through an inverted 0.8 numerical aperture 60x oil-immersion objective lens. The objective focus was first found by imaging the sample under bright-field illumination, then the sample was removed and the laser was focused at the ceiling (approximately 2 m beyond the sample location) for this placement of the objective. The sample was then replaced, and fluorescence was collected through a 629/56 nm band-pass filter by a SCMOS camera (Andor Zyla). Video was collected with an exposure of 8 ms and frame rates of 32 FPS for the fast component of the decay and 10 FPS for the slow component, at irradiances ranging from 2-200 W/cm². Fig. 6 shows a single frame from video collected at 19 W/cm².

2.2 Single molecule measurements

2.2.1 Sample preparation and single molecule imaging

FR was expressed in *E. coli* cells and purified by His-tag gravity chromatography, then flash frozen with liquid N₂ and stored at -80°C in dialysis buffer (150 mM NaCl, 50 mM Tris-HCL, pH 7.4).

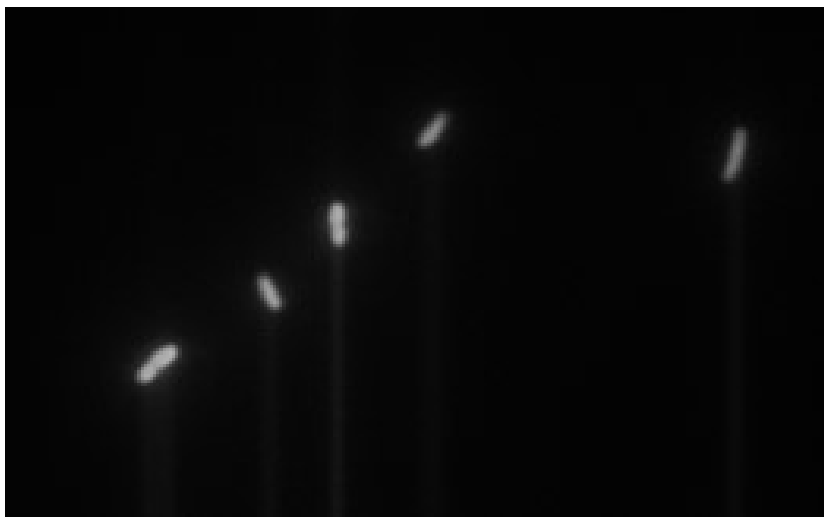


Figure 6: Single frame from video collected of *E. coli* cells expressing the RFP FusionRed.

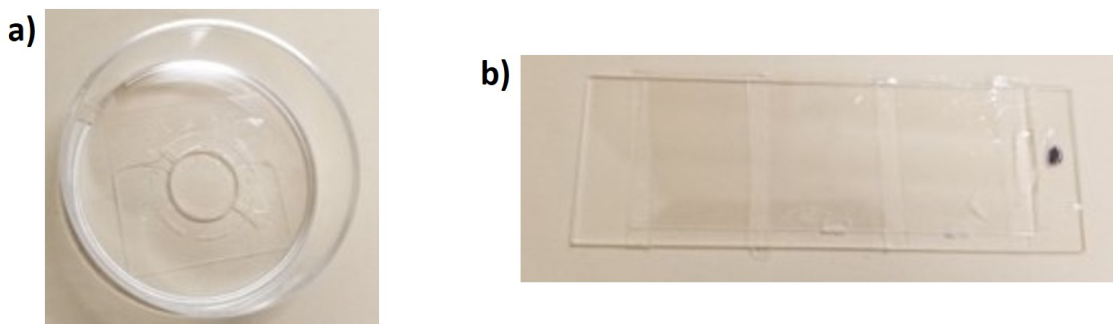


Figure 7: **a)** Original sample chamber, which did not provide a level imaging surface. **b)** Final sample chamber constructed by attaching a glass slide and coverslip together with double-sided tape.

Initially, sample chambers were built by punching holes in plastic petri dishes and gluing a glass coverslip over the hole through which to image (Fig. 7a), in an effort to replicate expensive commercial cell culture imaging dishes. This method was eventually discarded because the gluing process produced an imaging surface which was not level, making it difficult to focus. Finally, sample chambers were constructed by attaching a glass slide and glass coverslip together using thin strips of double-sided tape (Fig. 7b). Multiple strips could be used to produce multiple compartments on the same slide, in order to test different conditions, but more than three resulted in fast evaporation of the sample.

Though minimizing the presence of impurities is always important, it is of particular concern in single-molecule studies, where large numbers of observations of authentic

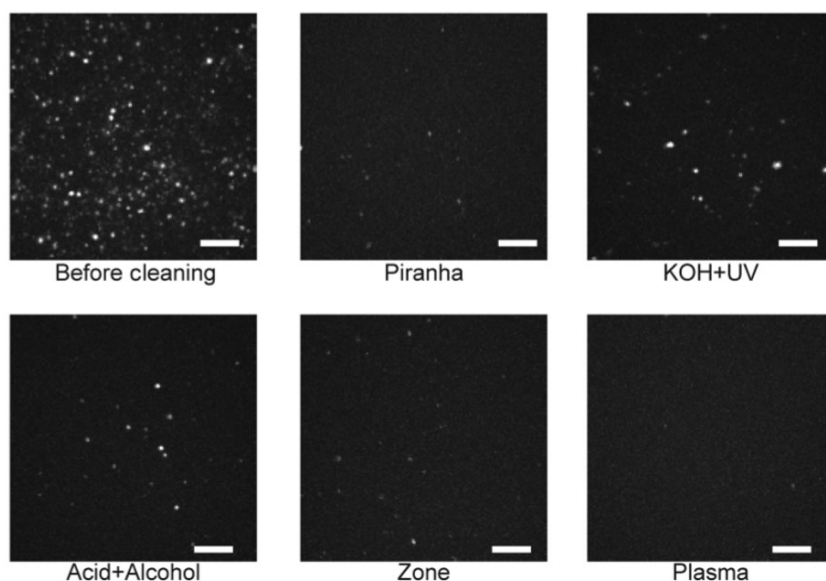


Figure 8: Comparison of cleaning methods for glass microscope slides [40]. Plasma cleaning is the most effective method for reducing contaminants.

individual fluorescent molecules are crucial. To this end, several methods were tested for cleaning the glass slides and coverslips used to make sample chambers. Eventually the most effective method was found to be plasma cleaning, wherein a reactive plasma species is created by applying high voltage to O_2 gas, and the energy released by this species breaks the bonds of organic surface contaminants, the fragments of which evaporate [39]. This result is corroborated in the literature [40]. A visual comparison of their various cleaning methods can be found in Fig. 8.

Before plasma cleaning, the slides and cover slips were cleaned with Alconox detergent and rinsed with deionized water, then soaked in methanol for at least an hour, in order to dislodge large contaminants. A container was designed and custom-built by the JILA machine shop for the purpose of holding slides and cover slips of the appropriate size inside the reactive ion etcher, so that they rested upright in grooves and both sides could be exposed to the plasma.

The sample chambers were constructed as described above and used within two days of plasma cleaning, to avoid recontamination. The sample was thawed, properly diluted, and loaded by slow ejection from a $200 \mu L$ micropipette (larger tip ejects too quickly, spilling FP solution onto the coverslip surface). It was determined that FP

concentrations greater than 300 pM produced crowding and poor signal-to-background ratio, while lower concentrations resulted in such sparse fields of view that it became difficult to find the correct focus height, and measurements yielded too few data points. Additionally, a washing procedure was developed in order to minimize the presence of FPs in solution, not stuck electrostatically to the glass imaging surface. After loading the sample into the chamber, it was left for 10-15 minutes (in the dark, to prevent photobleaching) to allow FPs to settle onto the imaging surface. Then a volume of dialysis buffer equal to 4-5 times the volume of loaded sample was flowed through the chamber. The liquid was slowly ejected by micropipette on one side of the chamber while filter paper was used to absorb the liquid flowing out from the other side. This washing procedure helped significantly to maximize signal-to-background ratios.

The samples were imaged using total internal reflection fluorescence (TIRF) microscopy on the same microscope set-up described for ensemble measurements. TIRF microscopy relies on the bending of light away from normal upon traveling from a higher index of refraction (n_1) medium to a lower index of refraction medium (n_2), as given by Snell's law [41]. At angles of incidence beyond the critical angle (θ_c), the light is totally internally reflected, and an evanescent wave propagates along the interface on the lower n side, with an amplitude which decays exponentially with distance into the medium. This phenomenon occurs when light propagates from the glass of a coverslip to the imaging solution, allowing for selective excitation of molecules within a few hundred nm of the surface [42]. The intensity of the evanescent field (I_e) is given in terms of the incident intensity (I), the ratio of indices of refraction ($n = \frac{n_2}{n_1}$), and the incident angle (θ) [41]:

$$I_e = I \frac{4(\cos\theta)^2(2(\sin\theta)^2 - n^2)}{n^4(\cos\theta)^2 + (\sin\theta)^2 - n^2} \quad (6)$$

Thus the evanescent field intensity can be several times greater than the incident intensity for incident angles just beyond the critical angle. A schematic of an objective-type TIRF microscopy system is found in Fig. 9. Irradiances for single-molecule studies were calculated using Eq. 6 after measuring incident power using a power meter and

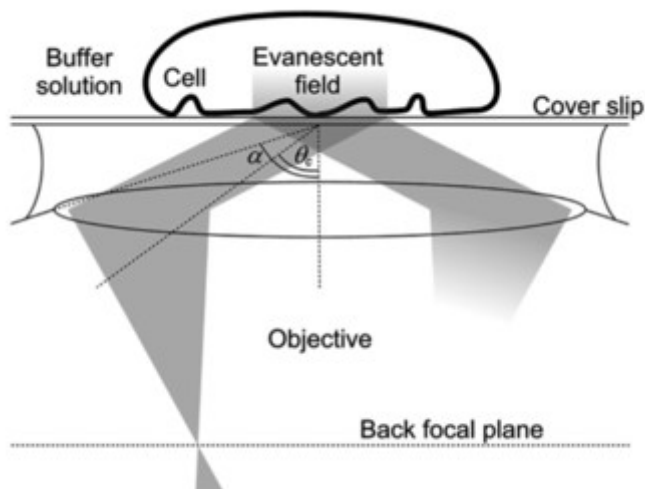


Figure 9: Schematic of TIRF system used for single-molecule imaging [41].

setting the angle of incidence for maximum contrast. The laser spot size was calculated to be $3.0 \times 10^{-4} \text{ cm}^2$. Videos of FR single-molecule blinking were recorded with 20 ms exposure and frame rate 32 FPS, at irradiances of 25-116 W/cm^2 .

2.2.2 Data analysis

All analysis was conducted using home-built programs in MATLAB. The elements of analysis were as follows:

Background subtraction: In each frame of each video, a background value was calculated as the average pixel value over the entire image. Though this average includes the bright spots as well as the background, the fraction of bright pixels in any frame is less than 10^{-5} , so their contribution can be neglected. Over an area roughly equal to $\frac{1}{16}$ of the image area, the average pixel value varied by less than 2% over the entire image, meaning that the background signal is fairly uniform within a single frame so subtraction of a single background value is valid. Between frames, however, the background value varied as much as 5%, validating the need for frame-specific background subtraction.

Spot identification: After frame-specific background subtraction, the brightest 1% of pixels were identified and adjacent pixels were grouped into fluorescent "spots" corresponding to single molecules. Spots consisting of one pixel were discarded, because real images of single molecules are larger.

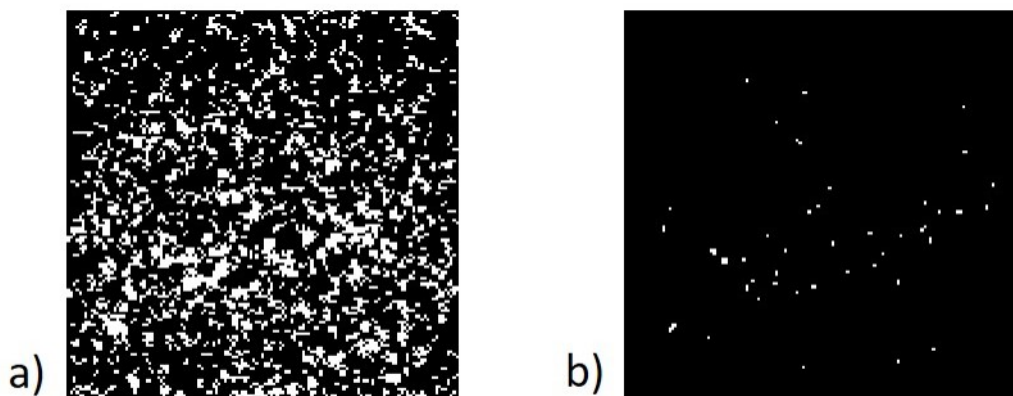


Figure 10: **a)** Locations of top 1% of pixels identified in all frames of a typical video, before filtering based on persistence. **b)** Locations of spots remaining after filtering based on persistence.

Removing redundancy: At this point, it would be easy to obtain fluorescent signal traces for each spot identified in each frame. However, this would generate a huge number of redundant signal traces, as each spot is likely identified in multiple frames. Complicating matters, for each spot, slightly different pixels may be identified in different frames. To get around this, a map was created of all pixels identified in all frames, and the fluorescence signal trace for each selected pixel was considered individually. Thus none of the traces are redundant, since they are from different locations. A map showing the locations of identified spots at this stage is found in Fig. 10(a).

Filtering based on persistence: Pixels which only appear bright for a few frames are likely not real single molecules stuck to the glass interface, but rather cosmic rays or molecules diffusing past in solution. To remove these cases, a selection filter was added to determine which of the selected pixels remain bright (in the top 1%) for some minimum number of frames. The pixels meeting this criteria were then recombined into spots if found adjacent to each other. A map showing identified spots from all frames remaining after this step is found in Fig. 10(b).

Manual visual filtering: The algorithm at this point had identified 40-200 spots in each video. The fluorescence traces from these spots were visually inspected, and only those with the best signal-to-background ratio were kept for analysis. Fig. 11 shows a typical array of fluorescence traces, and examples of traces which were chosen

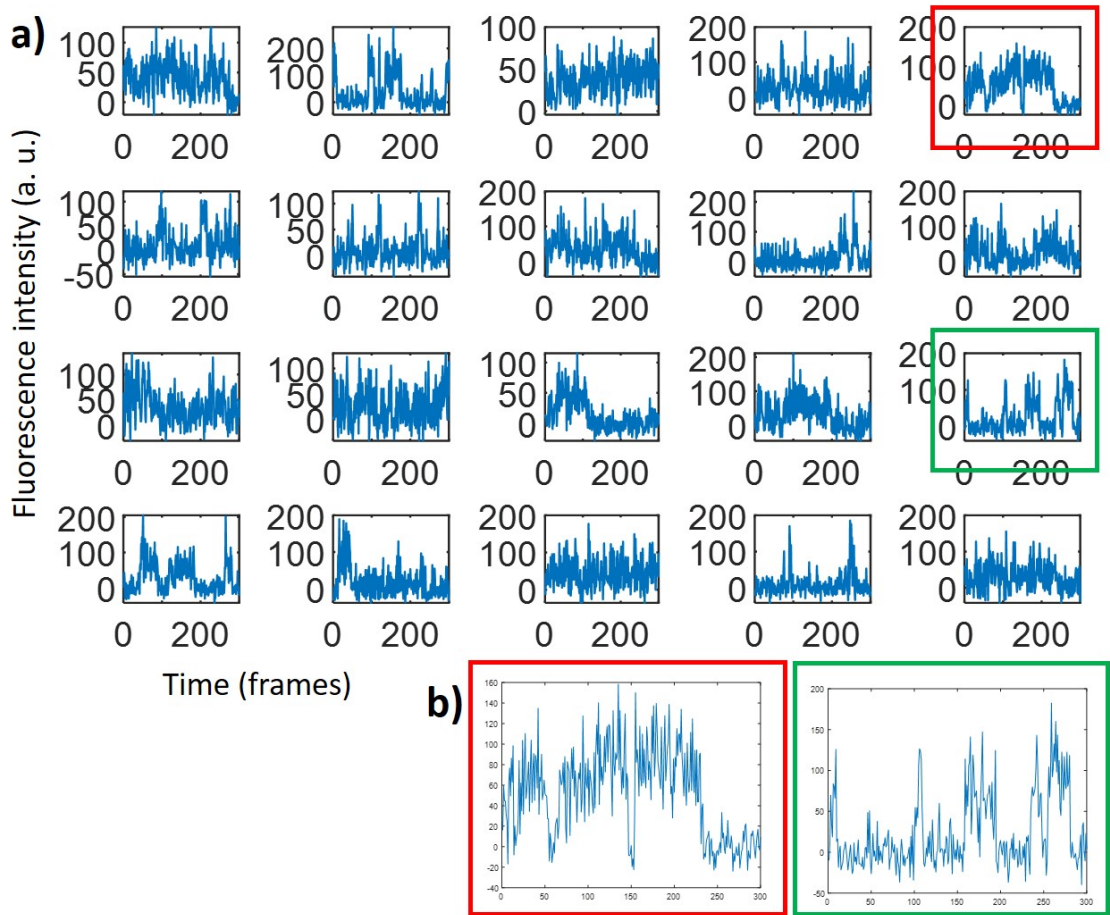


Figure 11: **a)** A typical array of a selection of fluorescence traces of spots identified in one video. **b)** Two examples of good spots subjectively chosen from this array.

from this array. Chosen traces exhibited unambiguous on/off transitions and relatively good signal-to-noise. Unfortunately, no other way could be determined at this point to algorithmically select these spots. However, this problem is well-suited for machine-learning methods, which would mitigate the need for subjective comparison.

Binarization of fluorescence traces into on and off states: If the experimental blinking data were similar to that obtained for GFP [21], then the determination of whether the FP is in the off or on state would be as simple as defining a signal cutoff, above which the FP is on and below which it is off. However, since FR is not as bright as GFP, signal-to-noise levels in the present experiment are significantly worse. The example blinking traces found in Fig. 11b can be compared to that in Fig. 4.

In order to account for the noise, for each selected trace, an average fluorescence intensity was calculated over increments of several frames (n_f). When the intensity

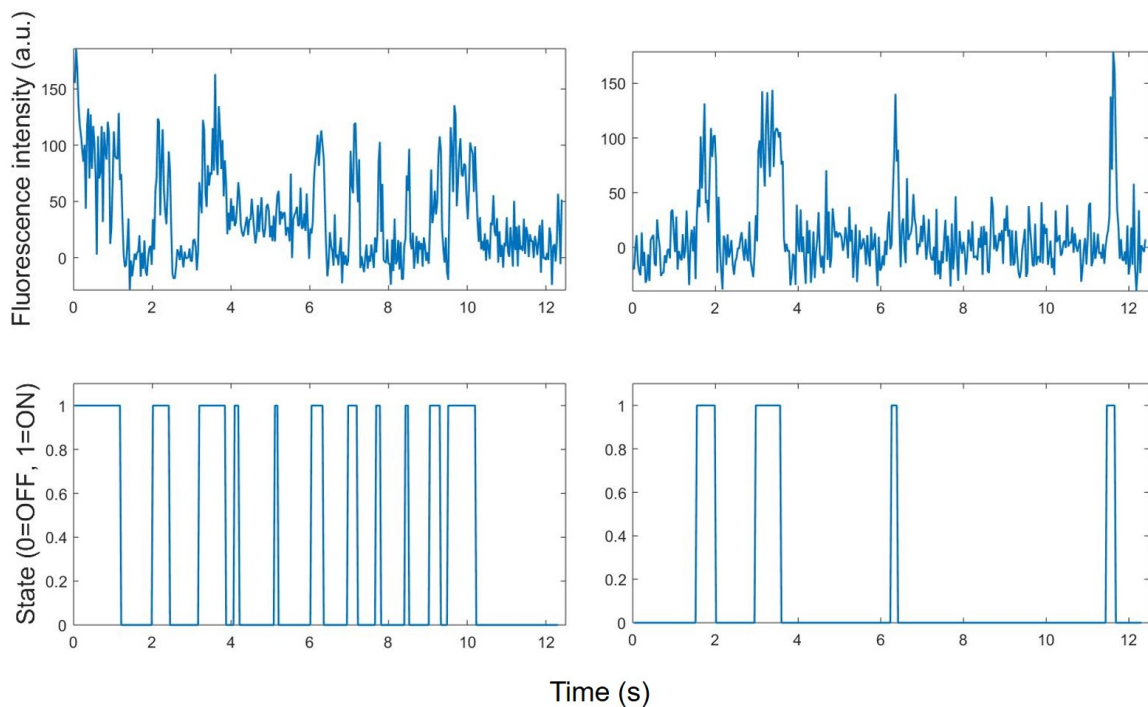


Figure 12: Results of binarization algorithm for two example fluorescent traces.

of a pixel averaged over a given frame plus the next n_f frames was higher than some threshold (t), the FP was considered to be on, and when lower, it was considered to be off. This way, if the intensity decreased slightly below t for a short time due to noise, it would not be considered a blink. This method produces a bias against short blinks, which should be considered when interpreting results. Different irradiances required different values of n_{frames} and t . Binarization results of two individual blinking traces are found in Fig. 12. For each trace, the last interval was excluded from analysis, whether on or off, as the actual duration of this interval is unknown since data collection ended.

At the lowest irradiance obtainable in the current TIRF microscope system (25 W/cm²), eight videos were collected of 300 frames each, in which only 71 suitable single-molecule fluorescence traces exhibiting blinking were identified. In future experiments, much more data should be collected.

3 Results and discussion

3.1 Ensemble fluorescence measurements

Ensemble fluorescence decay traces for FRM can be found in Fig. 13, illustrating the faster timescale of photobleaching at higher intensities. With similar data for FR at 19 W/cm², a biexponential fit was used to qualitatively determine the timescales of GSR and photobleaching, assuming that the fast decay corresponds to GSR and the long decay to photobleaching (Fig. 14, left). The resulting approximate time constants were 2.3 and 10.7 s, respectively, meaning that the processes are competitive. Accordingly, only the first 4 s of the decay was fit using the solution to Eq. 2 to extract k_{DSC} and k_{GSR} values of $5.6 \times 10^3 \text{ s}^{-1}$ and 0.11 s^{-1} , giving a GSR time constant of 9.1 s (Fig. 14, right). Despite good agreement between the fitting and experimental curves, the two fitted GSR time constants do not agree. This is because the 3-state model assumed no irreversible photobleaching, but there was experimentally a non-negligible photobleaching contribution. Thus the GSR time constant obtained by fitting the 3-state model was longer, and the DSC and GSR time constants obtained from the 3-state model fitting do not reflect their actual values.

3.2 Single-molecule fluorescence measurements

Normalized frequency distribution histograms for on and off times can be found in Fig. 15. The mean on and off times were 0.12 and 0.15 s, respectively. The predicted on and off times, based on the ensemble decay fitting and Eq. 4, were 0.15 and 9.0 s, respectively. The experimental and theoretical on times approximately agree, while the off times differ by over an order of magnitude. The discrepancy can be explained by two considerations. First, the contribution from photobleaching is non-negligible but not accounted for in the 3-state model, as previously discussed. Second, these histograms represent only 71 observed single molecules, which may not provide an accurate statistical result (in single-molecule literature, results are typically reported from hundreds or thousands of molecules).

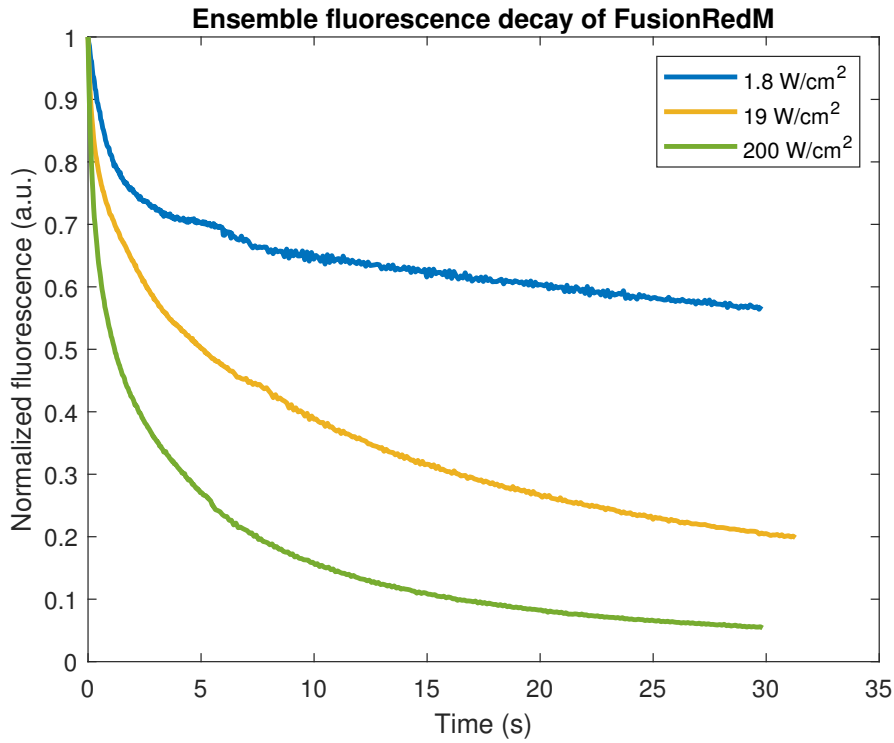


Figure 13: Ensemble fluorescence decay traces for FRM at a range of illumination intensities. At lower intensities, the decay is more biexponential, as the timescales of GSR and photobleaching differ significantly, while at higher intensities, the decay becomes closer to monoexponential.

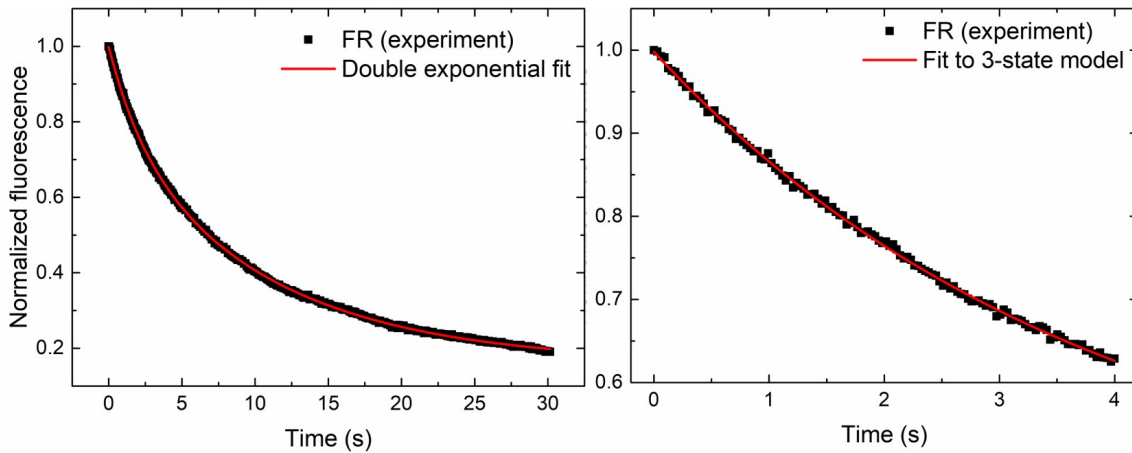


Figure 14: **Left:** Biexponential fit of FRM fluorescence decay, yielding time constants $\tau_{GSR}=2.3$ s and $\tau_{PB}=10.7$ s. **Right:** Fit to solution of 3-state model, yielding time constant $\tau_{GSR}=9.1$ s.

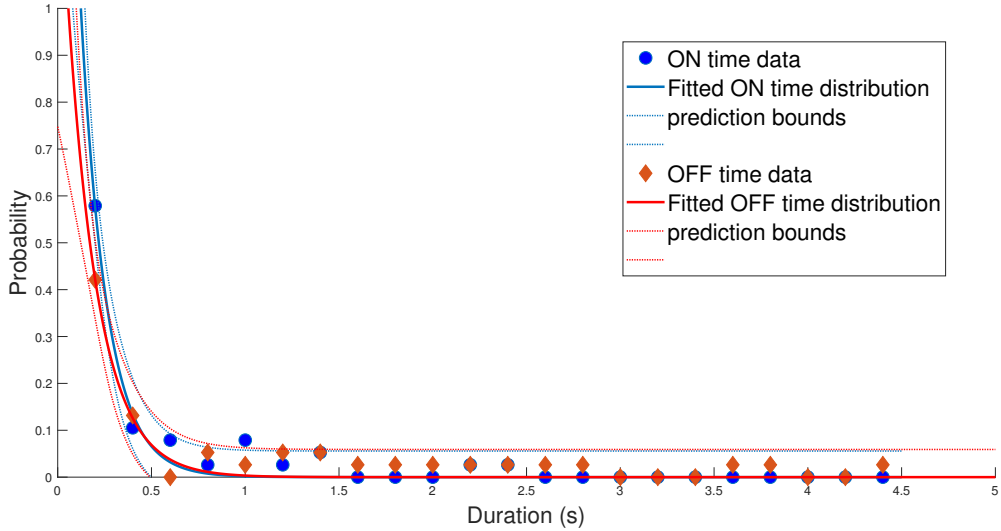


Figure 15: Frequency distribution histograms for on and off times during FR blinking at 25 W/cm^2 irradiance.

Another consideration in interpretation of these results is that the blinking spots were selected by applying the criteria of persistence for 4 frames continuously ($n_{frames} = 4$). This biases the collected data against short blinks on, and in fact the average experimental on time is consistent with a 4-frame persistence, based on the time interval of 31 ms between frames. Thus the persistence filter may be limiting the accuracy of on and off times at small time intervals. Considering these factors, the agreement in DSC time constant could be coincidence, or could indicate that the DSC time constant is not as sensitive to photobleaching as the GSR time constant, since the timescales between DSC and photobleaching differ by orders of magnitude.

3.3 Conclusion and future directions

The value of this work is primarily in establishing a protocol for observing and analyzing blinking behavior in RFPs at the single-molecule level, and in attempting to obtain the crucial photophysical parameters for super-resolution imaging techniques by bridging ensemble and single-molecule measurements. The blinking results discussed here are preliminary. Future studies will need to collect more data in order to construct meaningful on/off time histograms. A neutral-density filter may be used to access lower irradiance regimes where photobleaching can be neglected during the observation time

as required by imaging applications. With single molecule blinking data and ensemble fluorescence decay data under proper illumination conditions, parameters obtained by fitting according to the 3-state model can be compared to the experimental on and off time intervals to validate or refute the model. The work done here to develop a protocol for sample preparation and an algorithm for analysis of noisy fluorescence blinking data can be used as a foundation for the future study of promising RFPs and nIRFPs.

References

- [1] Euskirchen G Ward WW Chalfie M, Tu Y and Prasher DC. Green fluorescent protein as a marker for gene expression. *Science*, 263(February):802–805, 1994.
- [2] Martin Chalfie. Green Fluorescent Protein GFP: Lighting Up Life (Nobel Lecture)**. 2008.
- [3] B. N. G. Giepmans, Stephen R Adams, Mark H Ellisman, and Roger Y Tsien. The Fluorescent Toolbox for Assessing Protein Location and Function. *Science*, 312(5771):217–224, 4 2006.
- [4] R Y Tsien. The green fluorescent protein. *Annual review of biochemistry*, 67:509–44, 1998.
- [5] J. Lippincott-Schwartz. Development and Use of Fluorescent Protein Markers in Living Cells. *Science*, 300(5616):87–91, 2003.
- [6] Asako Sakaue-Sawano, Hiroshi Kurokawa, Toshifumi Morimura, Aki Hanyu, Hiroshi Hama, Hatsuki Osawa, Saori Kashiwagi, Kiyoko Fukami, Takaki Miyata, Hiroyuki Miyoshi, Takeshi Imamura, Masaharu Ogawa, Hisao Masai, and Atsushi Miyawaki. Visualizing Spatiotemporal Dynamics of Multicellular Cell-Cycle Progression. *Cell*, 132(3):487–498, 2008.
- [7] Clare E. Rowland, Carl W. Brown, Igor L. Medintz, and James B. Delehanty. Intracellular FRET-based probes: A review. *Methods and Applications in Fluorescence*, 3(4), 2015.
- [8] F. Meng and F. Sachs. Orientation-based FRET sensor for real-time imaging of cellular forces. *Journal of Cell Science*, 125(3):743–750, 2012.
- [9] Xiaokun Shu, Nathan C. Shaner, Corinne A. Yarbrough, Roger Y. Tsien, and S. James Remington. Novel Chromophores and Buried Charges Control Color in mFruits. *Biochemistry*, 45(32):9639–9647, 8 2006.

- [10] Premashis Manna. Development and Characterization of Improved Red Fluorescent Protein Variants. *Chemistry & Biochemistry Graduate Theses & Dissertations*, 1 2018.
- [11] Erik A. Rodriguez, Robert E. Campbell, John Y. Lin, Michael Z. Lin, Atsushi Miyawaki, Amy E. Palmer, Xiaokun Shu, Jin Zhang, and Roger Y. Tsien. The Growing and Glowing Toolbox of Fluorescent and Photoactive Proteins. *Trends in Biochemical Sciences*, 42(2):111–129, 2 2017.
- [12] I. I. Shemiakina, G. V. Ermakova, P. J. Cranfill, M. A. Baird, R. A. Evans, E. A. Souslova, D. B. Staroverov, A. Y. Gorokhovatsky, E. V. Putintseva, T. V. Gorodnicheva, T. V. Chepurnykh, L. Strukova, S. Lukyanov, A. G. Zaraisky, M. W. Davidson, D. M. Chudakov, and D. Shcherbo. A monomeric red fluorescent protein with low cytotoxicity. *Nature Communications*, 3:1204–1207, 2012.
- [13] Premashis Manna, Sheng-Ting Hung, Srijit Mukherjee, Pia Friis, David M. Simpson, Maria N. Lo, Amy E. Palmer, and Ralph Jimenez. Directed evolution of excited state lifetime and brightness in FusionRed using a microfluidic sorter. *Integrative Biology*, 10(9):516–526, 9 2018.
- [14] Natalia V. Klementieva, Anton I. Pavlikov, Alexander A. Moiseev, Nina G. Bozhanova, Natalie M. Mishina, Sergey A. Lukyanov, Elena V. Zagaynova, Konstantin A. Lukyanov, and Alexander S. Mishin. Intrinsic blinking of red fluorescent proteins for super-resolution microscopy. *Chemical Communications*, 53(5):949–951, 2017.
- [15] Amy E Palmer, Xiaokun Shu, Jin Zhang, and Roger Y Tsien. The growing and glowing toolbox of fluorescent and photoactive proteins. *Trends in Biochemical Science*, 42(2):111–129, 2018.
- [16] Joseph R. Lakowicz, editor. *Principles of Fluorescence Spectroscopy*. Springer US, Boston, MA, 2006.
- [17] Daniel Schroeder. *Thermal Physics*. Addison Wesley Longman, 2000.

- [18] Martin Andresen, Andre C Stiel, Simon Trowitzsch, Gert Weber, Christian Eggeling, Markus C Wahl, Stefan W Hell, and Stefan Jakobs. Structural basis for reversible photoswitching in Dronpa. *Proceedings of the National Academy of Sciences of the United States of America*, 104(32):13005–9, 8 2007.
- [19] Russell B. Vegh, Ksenia B. Bravaya, Dmitry A. Bloch, Andreas S. Bommarius, Laren M. Tolbert, Michael Verkhovsky, Anna I. Krylov, and Kyril M. Solntsev. Chromophore Photoreduction in Red Fluorescent Proteins Is Responsible for Bleaching and Phototoxicity. *The Journal of Physical Chemistry B*, 118(17):4527–4534, 5 2014.
- [20] Th Basche, S Kummer, and C Brauchle. Direct spectroscopic observation of quantum jumps of a single molecule. *Nature*, 373(6510), 1995.
- [21] Robert M Dickson, Andrew B Cubitt, and Roger Y Tsien. On / off blinking and switching behaviour of single molecules of green fluorescent protein. *Nature*, 388(July):355–358, 1997.
- [22] S. J. Strickler and Robert A. Berg. Relationship between Absorption Intensity and Fluorescence Lifetime of Molecules. *The Journal of Chemical Physics*, 37(4):814–822, 8 1962.
- [23] Wai-Tak Yip, Dehong Hu, Ji Yu, David A. Vanden Bout, , and Paul F. Barbara*. Classifying the Photophysical Dynamics of Single- and Multiple-Chromophoric Molecules by Single Molecule Spectroscopy. 1998.
- [24] M. Riedl. *Optical Design Fundamentals for Infrared Systems*. SPIE, Bellingham, WA, 2nd edition, 2001.
- [25] Max. Born. *Principles of Optics*. Elsevier Science, 1980.
- [26] Jennifer Lippincott-Schwartz and George H. Patterson. Photoactivatable fluorescent proteins for diffraction-limited and super-resolution imaging. *Trends in Cell Biology*, 19(11):555–565, 11 2009.

- [27] Eric Betzig, George H Patterson, Rachid Sougrat, O Wolf Lindwasser, Scott Olenych, Juan S Bonifacino, Michael W Davidson, Jennifer Lippincott-Schwartz, and Harald F Hess. Imaging intracellular fluorescent proteins at nanometer resolution. *Science (New York, N.Y.)*, 313(5793):1642–5, 9 2006.
- [28] Samuel T. Hess, Thanu P.K. Girirajan, and Michael D. Mason. Ultra-High Resolution Imaging by Fluorescence Photoactivation Localization Microscopy. *Biophysical Journal*, 91(11):4258–4272, 12 2006.
- [29] Michael J Rust, Mark Bates, and Xiaowei Zhuang. Sub-diffraction-limit imaging by stochastic optical reconstruction microscopy (STORM). *Nature Methods*, 3(10):793–796, 10 2006.
- [30] Julie Biteen and Katherine A. Willets. Introduction: Super-Resolution and Single-Molecule Imaging. *Chemical Reviews*, 117(11):7241–7243, 6 2017.
- [31] George Patterson, Michael Davidson, Suliana Manley, and Jennifer Lippincott-Schwartz. Superresolution Imaging using Single-Molecule Localization. *Annual Review of Physical Chemistry*, 61:345–367, 2010.
- [32] T Dertinger, R Colyer, G Iyer, S Weiss, and J Enderlein. Fast, background-free, 3D super-resolution optical fluctuation imaging (SOFI). *Proceedings of the National Academy of Sciences of the United States of America*, 106(52):22287–92, 12 2009.
- [33] Kevin M. Dean, Jennifer L. Lubbeck, Jennifer K. Binder, Linda R. Schwall, Ralph Jimenez, and Amy E. Palmer. Analysis of Red-Fluorescent Proteins Provides Insight into Dark-State Conversion and Photodegradation. *Biophysical Journal*, 101(4):961–969, 8 2011.
- [34] Premashis Manna and Ralph Jimenez. Time and frequency-domain measurement of ground-state recovery times in red fluorescent proteins. *Journal of Physical Chemistry B*, 119(15):4944–4954, 2015.
- [35] P Schuille, S Kummer, A A Heikal, W E Moerner, and W W Webb. Fluorescence correlation spectroscopy reveals fast optical excitation-driven intramolecular

- dynamics of yellow fluorescent proteins. *Proceedings of the National Academy of Sciences of the United States of America*, 97(1):151–6, 1 2000.
- [36] W E Moerner and L Kador '. Optical Detection and Spectroscopy of Single Molecules in a Solid. Technical report, 1989.
- [37] E. Brooks Shera, Newton Seitzinger, Lloyd Davis, Richard Keller, and Steven Soper. Detection of single fluorescent molecules. *Chemical Physics Letters*, 174(6):553–557, 1990.
- [38] W E Moerner and Michel Orrit. Illuminating Single Molecules in Condensed Matter. *Science*, 283:1670–1676, 1999.
- [39] Hidenori Sekiya and Kenji Shirakawa. Plasma processing apparatus and plasma cleaning method. 8 1992.
- [40] Janel L Davis and Hao F Zhang. Method to identify and minimize artifacts induced by fluorescent impurities in single-molecule localization microscopy. 23(10), 2019.
- [41] M. L. Martin-Fernandez, C. J. Tynan, and S. E.D. Webb. A 'pocket guide' to total internal reflection fluorescence. *Journal of Microscopy*, 252(1):16–22, 2013.
- [42] Kenneth N. Fish. Total Internal Reflection Fluorescence (TIRF) Microscopy. In *Current Protocols in Cytometry*, volume 50, pages 1–12. John Wiley & Sons, Inc., Hoboken, NJ, USA, 10 2009.